Biochemical and Biophysical Research Communications 478 (2016) 1087–1092

Contents lists available at ScienceDirect

Biochemical and Biophysical Research Communications

journal homepage: www.elsevier.com/locate/ybbrc

Microscopic analysis of Orai-mediated store-operated calcium entry in cells with experimentally altered levels of amyloid precursor protein

Tomasz Wegierski*, Kinga Gazda, Jacek Kuznicki

Laboratory of Neurodegeneration, International Institute of Molecular and Cell Biology, 02-109, Warsaw, Poland

ARTICLE INFO

Article history:
Received 5 August 2016
Accepted 11 August 2016
Available online 12 August 2016

Keywords:
Calcium signaling
Amyloid precursor protein
Alzheimer's disease
Store-operated calcium entry
Capacitative calcium entry
Orai

ABSTRACT

Familial Alzheimer's disease (FAD)-causing mutations in presenilins were shown to alter intracellular calcium dynamics, including store-operated calcium entry (SOCE). However, the involvement of FAD-linked amyloid precursor protein (APP) in SOCE remains controversial. Here, we used gain-of-function and loss-of-function approaches to shed light on this issue. We found that Jurkat cells, which exhibit prominent SOCE mediated by Orai channels, maintain low APP levels. The ectopic expression of APP, either with wildtype sequence or FAD-causing Swedish mutation, had no effect on SOCE induced by calcium store depletion with cyclopiazonic acid (CPA). The overproduction of C99 fragments, mimicking amyloidogenic processing of APP, also had no effect. Moreover, there was no alteration in the CPA-evoked SOCE upon APP knockdown in HeLa cells, which natively express 100-fold more APP than Jurkat cells. Consistently, we found no evidence for APP-dependent changes in the mRNA or protein levels of main SOCE components. Altogether, these results suggest that APP does not modulate Orai-dependent SOCE following quantitative calcium store depletion.

1. Introduction

Alzheimer's disease (AD) is the most common neurodegenerative disorder. Early-onset familial AD (FAD) cases are caused by mutations in the genes that encode presenilin-1 (PS1), presenilin-2, and amyloid precursor protein (APP) [1,2]. Presenilins constitute the enzymatic component of γ-secretase, which processes various integral membrane proteins, including APP [3]. The amyloidogenic processing of APP begins with cleavage by β-secretase, yielding the C99 fragment [2]. Subsequent cleavage by γ-secretase leads to the formation of Aβ peptides and APP intracellular C-terminal domain (AICD). Alternatively, in non-amyloidogenic processing, cleavage by α-secretase precludes β-amyloid formation and gives rise to the C83 fragment. FAD mutations favor amyloidogenic processing and an increase in $A\beta_{42}/A\beta_{40}$ ratios [1].

The prevalent β-amyloid cascade hypothesis of AD assumes that the accumulation of Aβ plaques or oligomers is the pathogenic factor. However, all Aβ-targeting treatments have failed in clinical trials [4]. One of the alternative hypotheses suggests that the dysregulation of neuronal calcium (Ca^{2+}) homeostasis is the major cause of AD [4–6]. This calcium hypothesis of AD is supported by experimental work in animal and cell models. Importantly, FAD-PS1 cells, both of neuronal and non-neuronal origin, have been shown to exhibit enhanced Ca^{2+} release through inositol 1,4,5-trisphosphate (IP_3) receptors from the endoplasmic reticulum (ER), which is the main intracellular Ca^{2+} store [7,8]. This upregulation of ER Ca^{2+} signaling might lead to aberrant synaptic transmission and neuronal cell death. The work in many laboratories, including ours, has shown that PS1 FAD mutations also reduce store-operated Ca^{2+} entry (SOCE) [9–13]. Conversely, the attenuation of γ-secretase activity increases SOCE [11,12,14,15]. SOCE is triggered by ER Ca^{2+} store depletion, resulting in subsequent Ca^{2+} influx from the extracellular space [16]. The ER Ca^{2+} sensing function is provided by closely-related stromal interaction molecule 1 (STIM1) and STIM2 proteins. Upon Ca^{2+} depletion from the ER, STIM proteins oligomerize and translocate to the ER-plasma membrane junctions, where they activate highly selective Ca^{2+} channels that are composed of Orai1-3 subunits [16]. In some cells, notably in astrocytes, channels from the canonical transient receptor potential (TRPC) family may contribute to SOCE [17]. STIM1/Orai1-mediated SOCE constitutes the major Ca^{2+} entry mechanism in non-excitable cells, and accumulating evidence points to an important role of SOCE also in neurons [18]. In particular, recent work demonstrated that neuronal SOCE is required for spine

* Corresponding author.
E-mail address: twegierski@iimcb.gov.pl (T. Wegierski).

http://dx.doi.org/10.1016/j.bbrc.2016.08.072

survival, a process that is disrupted in FAD knock-in mouse models [13,19].

Compared with PS1, the involvement of APP and its FAD mutants in intracellular Ca^{2+} homeostasis has been less studied. Their Ca^{2+}-related functions appear to be carried out by γ-secretase processed products. Aβ oligomers may increase Ca^{2+} entry, whereas AICD was implicated in ER Ca^{2+} signaling [5]. The role of APP in SOCE is confusing. Ablation of APP expression was reported to reduce SOCE in astrocytes [20]. APP FAD mutations were shown both to enhance SOCE [21] and to attenuate it [19]. Others have found no evidence that APP, APP FAD mutants, or Aβ is involved in the regulation of SOCE [9,11,22,23]. The aim of the present study was to reinvestigate the role of APP, APP FAD mutants and cleavage products in cells with proven Orai-dependent SOCE.

2. Materials and methods

2.1. Reagents and plasmids

Cyclopiazonic acid (CPA), DAPT, polybrene and poly-L-lysine (PLL) were obtained from Sigma-Aldrich. Fura-2/AM and Fura-4F/AM were obtained from Life Technologies. Human *APP* and *ORAI1* coding sequences originated from Addgene plasmids #30137, #30145 and #22754, and were cloned MluI-NotI into a modified pLVTH vector (Addgene #12262), in which eGFP and the H1 promoter were replaced with an IRES-PURO-WPRE cassette. The short-hairpin RNAs (shRNA; see Supplementary materials) were cloned into a pSUPER.retro vector (Oligoengine) or into a modified pLVTH vector, in which eGFP was replaced with a puromycin selection marker.

2.2. Cell cultures, virus production, and transduction

Jurkat E6-1, 293T/17 and HeLa cells were obtained from ATCC. 293T/17 and HeLa cells were grown in Dulbecco's Modified Eagle Medium and Jurkat cells in RPMI-1640 supplemented with 10 mM HEPES. All media contained 10% FBS. For virus production, 293T/17 cells were transfected with transfer and helper plasmids using the Ca^{2+}-phosphate method. Supernatants were collected 48 h after transfection, filtered through 0.45-μm cellulose acetate membranes and concentrated in Vivaspin 100-kDa units (Sartorius) in a swing-out rotor at 1,000×*g*. Functional viral titers were determined by transducing HeLa cells with serial dilutions of viral preparations. Cells were transduced in the presence of 4–8 μg/ml polybrene and selected with 1–2 μg/ml (HeLa) or 0.5 μg/ml (Jurkat) puromycin.

2.3. qPCR

RNA was isolated using the RNeasyPlus Mini kit (Qiagen). cDNAs were produced with SuperScript III Reverse Transcriptase (Life Technologies) and amplified (20 ng input RNA) using a 7900HT Real-Time PCR system (Applied Biosystems) with SYBR Green chemistry. For each primer pair (see Supplementary materials), a standard curve was prepared using serial dilutions of cDNAs. Analyzed mRNAs were normalized to *GAPDH* mRNAs, and relative levels were calculated using SDS 2.4 software. One *n* is defined as one independent RNA/cDNA preparation quantified 1–2 times by qPCR.

2.4. Measurements of SOCE

Cells attached on PLL-coated coverslips were loaded with Fura-2/AM or Fura-4F/AM in bath solution containing: 150 mM NaCl, 6 mM KCl, 1 mM $MgCl_2$, 2 mM $CaCl_2$, 10 mM glucose, 10 mM HEPES, pH 7.4. SOCE measurements were performed under perfusion with bath solution at 25 °C. Stores were depleted with Ca^{2+}-free bath solution supplemented with 20 μM CPA and (for HeLa cells) 0.5 mM EGTA. One *n* is defined as one measurement. For more details, see Supplementary methods.

2.5. FACS

Cells were washed in PBS and fixed with 2% paraformaldehyde in PBS. Blocking was performed in PBS containing 2% normal donkey serum and 0.2% saponin. The cells were stained with Y188 antibodies (1:500) in blocking solution, and washed two times in PBS. Subsequently, they were stained with Alexa Fluor 488-conjugated antibodies (1:1000) in blocking solution and washed two times in PBS. One reaction contained 1×10^6 cells. The signals were collected using a FACSCalibur flow cytometer (BD Biosciences). Data were analyzed using Flowing Software.

2.6. Statistical analysis

The data were analyzed in Excel or GraphPad Prism using two-tailed unpaired or one-sample *t*-test, as indicated. The calculated mean values are shown as bars with standard errors. Values of $p < 0.05$ were considered statistically significant.

3. Results

3.1. Jurkat cells express the APP gene at low levels

Inspection of the gene expression databases revealed that *APP* is abundantly expressed with the exception of leukocytes. Although some studies have reported detectable *APP* mRNA levels in T-cells [24], especially following stimulation, others found no evidence for APP presence in lymphocytes [25]. By screening various cultured cell lines, we found that Jurkat cells, which originated from a patient with acute T-cell leukemia, apparently lacked any APP. Neither of two established APP antibodies, 22C11 (which recognizes the N-terminal extracellular domain) and Y188 (which recognizes the intracellular C-terminal tail), detected full-length APP in lysates that were prepared from Jurkat cells, whereas both antibodies clearly indicated APP presence in two commonly used cell lines, HeLa and HEK 293T/17 (Fig. 1A). The lack of APP in Jurkat cell lysates may result from very fast proteolysis or low gene expression. Therefore, *APP* expression was quantified by qPCR using two primer pairs that are predicted to anneal to all known splicing isoforms, including the L-APP isoform that was found in T-cells [24]. Both primer pairs gave very consistent results for *APP* mRNA levels in Jurkat cells, with 95% confidence intervals of 0.37–1.18% and 0.34–1.15% for each primer pair, respectively, for the levels that were calculated for HeLa cells (Fig. 1B). The results allowed us to conclude that *APP* gene expression in Jurkat cells was two orders of magnitude lower than in HeLa cells and is likely the main reason for the undetectable APP signal in Jurkat cell lysates. Therefore, Jurkat cells were deemed an appropriate system for further functional studies with overexpressed APP variants, because it avoids interference from endogenously produced APP.

3.2. Generation of Jurkat cell lines that stably produce ectopic APP

To generate cell lines stably producing APP variants, Jurkat cells were transduced with viruses that carried cDNAs coding for APP (isoform 695, a predominant isoform in neuronal cells), APP with the K670N/M671L Swedish double mutation (APP_{SWE}), or empty cassette, as control. The Swedish mutation is known to facilitate processing at the β-site, thereby favoring the amyloidogenic

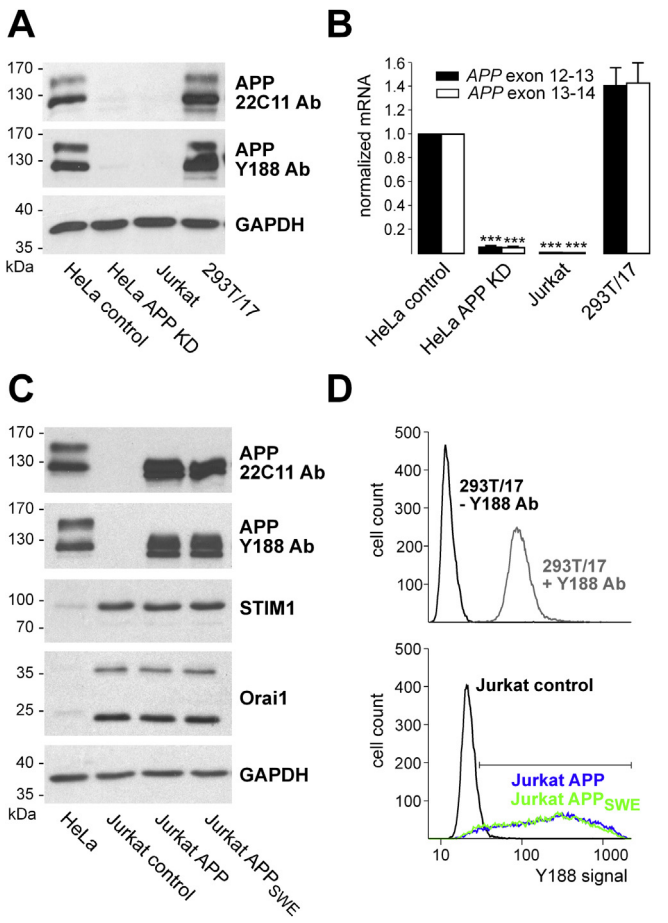

Fig. 1. Generation of Jurkat cell lines stably producing APP. (**A**) Immunoblot of endogenous APP in Jurkat, 293T/17, and HeLa cells carrying *APP*-targeting shRNA (APP KD) or control shRNA. (**B**) qPCR analysis of relative *APP* mRNA levels in cells presented in (A). Differences from the reference level of 1 set for HeLa control cells were analyzed using one-sample *t*-test ($n = 4$ each). Significant differences are marked with asterisks (***$p < 0.001$). (**C**) Immunoblot of APP, Orai1, and STIM1 in Jurkat cells stably expressing *APP*, APP_{SWE} or an empty cassette (control), compared with wildtype HeLa cells. (**D**) FACS analysis of Y188-labeled Jurkat APP cells and APP_{SWE} cells. Y188-labeled and mock-labeled 293T/17 cells were analyzed in parallel to set a threshold for Y188-positive cells (horizontal line). The x-axis of both histograms shows the Y188 signal normalized to cell size (FL1-H/FSC) on a logarithmic scale.

pathway [1,2]. Immunoblot analysis revealed the successful production of both APP variants in Jurkat cells at similar levels (Fig. 1C). As expected, overproduced APP migrated faster than the native protein in HeLa cells, which likely represents a non-neuronal 751 or 770 isoform. Neither APP variant affected steady-state levels of endogenous STIM1 or Orai1 proteins, which were clearly more abundant in all three Jurkat cell lines than in wildtype HeLa cells (Fig. 1C).

Subsequently, Jurkat cells were labeled with Y188 antibody to analyze APP levels in individual cells using fluorescence-activated cell sorting (FACS; Fig. 1D). In parallel, 293T/17 cells that were labeled with the same antibody or mock-labeled were analyzed to distinguish between APP-positive and APP-negative cell populations. With the threshold set such that all Y188-labeled 293T/17 cells were regarded as APP-positive, 95% of the Jurkat APP cells and 93.5% of the Jurkat APP_{SWE} cells were counted as APP-positive, with the median Y188 signal 2.8- or 2.5-times higher than the median signal in 293T/17 cells, respectively. Only 7.5% of the Jurkat control cells were counted as APP-positive, which likely reflects nonspecific binding of Y188 antibody in these cells. Altogether, these results demonstrate efficient introduction and expression of the *APP* cDNAs into Jurkat cells.

3.3. Overexpression of APP or APP_{SWE} in Jurkat cells has no effect on SOCE upon complete depletion of ER Ca^{2+} stores

T-cells are capable of substantial SOCE, which not only refills Ca^{2+} stores but also has important signaling functions [16,26]. To investigate whether APP has any effect on Ca^{2+} influx through store-operated channels (SOCs), we utilized an established microscopic method to measure intracellular Ca^{2+} dynamics in individual cells. The transduced Jurkat cells were loaded with the low-affinity Ca^{2+} sensor Fura-4F. This probe was chosen for use in Jurkat cells rather than the widely used high-affinity probe Fura-2 to avoid saturation of Ca^{2+} signals during SOCE transients. Subsequently, the cells were perfused with a Ca^{2+}-free bath solution containing 20 μM CPA (an inhibitor of SERCA) to fully deplete ER Ca^{2+} stores, and a bath solution with 2 mM Ca^{2+} was finally reapplied to initiate Ca^{2+} influx. This protocol aimed at optimal conditions for measuring SOCE, independent of ER Ca^{2+} filling state. Compared with control Jurkat cells, neither APP-producing cells nor APP_{SWE}-producing cells presented a significantly different SOCE response, quantified as the amplitude of the rise in intracellular [Ca^{2+}] or the maximal measured influx rate (Fig. 2A). The presence of APP variants also did not affect SOCE decline rates, indicating unchanged Ca^{2+} extrusion mechanisms in responding cells (Supplementary Fig. 1A). To confirm the dependence of SOCE responses on Orai channels, the measurements were also conducted on Jurkat cells that stably produced Orai1 with the E106Q mutation. This pore mutant exerts a dominant-negative effect (Orai1 DN) on Orai1 channels and presumably also on Orai2 and Orai3 channels [27]. Compared with control cells, Jurkat cells with Orai1 DN exhibited virtually no SOCE response, quantified by its amplitude or maximal influx rate (Fig. 2B). Altogether, these results indicate that neither APP nor APP_{SWE} affected SOCE in Jurkat cells, and SOCE depended on Ca^{2+} influx through Orai channels.

3.4. Overexpression of C99 or $C99_{IND}$ in Jurkat cells does not affect STIM1/Orai1 levels or SOCE

Oligomeric β-amyloid species, which are derived from APP C99 fragments, have been implicated in increasing Ca^{2+} entry [5]. However, the immunoblot analysis of small APP fragments from Jurkat APP_{SWE} cells indicated the presence of the 11-kDa band, corresponding to the α-processed C83 product, which could be clearly detected only upon γ-secretase inhibition with DAPT (Fig. 3A). The β-processed C99 fragment was undetectable in lysates from these cells, suggesting inefficient cleavage by β-secretase and/or fast further processing. Therefore, two new cell lines were prepared that expressed C99 cDNA with wildtype sequence or an Indiana mutation (V717F). The Indiana mutation is known to increase the β42/β40 ratio [1], and $C99_{IND}$ cells were expected to present potential differences in Ca^{2+}-related functions of these β-amyloid species. For both cell lines, only the 14-kDa band was detected in lysates from untreated cells, indicating successful production of C99 (Fig. 3B). The treatment of Jurkat C99 cells with DAPT increased the levels of C99 and, especially, C83, demonstrating that overproduced C99 can be further processed by α- and γ-secretases (Fig. 3A). The overproduction of C99 or $C99_{IND}$ did not affect the levels of STIM1 or Orai1 proteins (Fig. 3B). Because cleavage of C99 by γ-secretase liberates AICD, which was implicated in transcriptional regulation [5], the *STIM1* and *ORAI1* mRNA levels were quantified by qPCR. Compared with control cells, no significant differences were detected for C99 or $C99_{IND}$ cells (Fig. 3C). The cells were subsequently used to measure Ca^{2+} influx

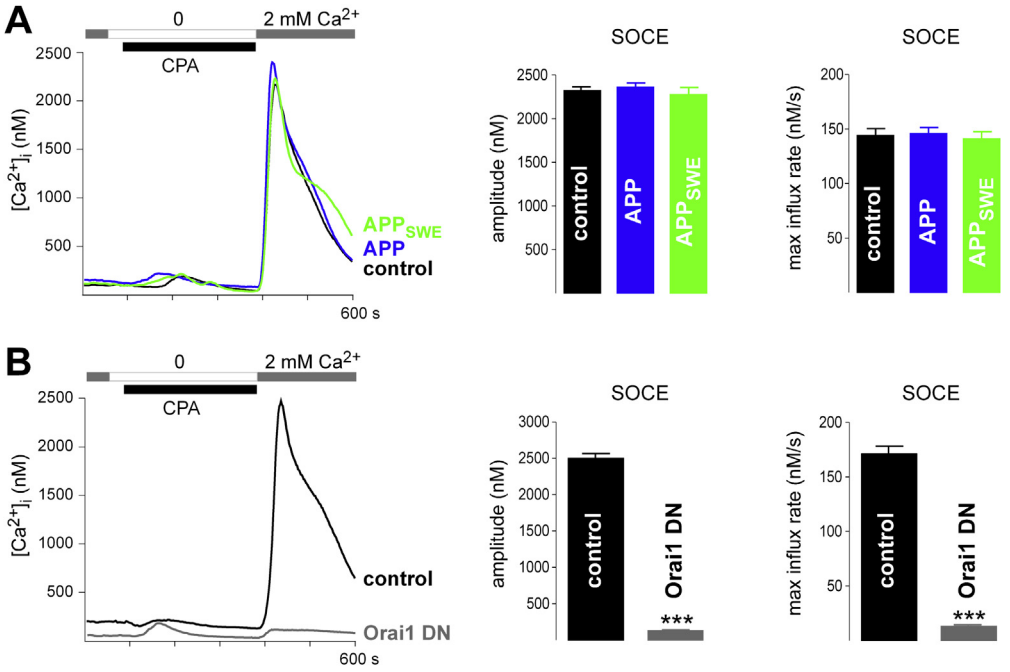

Fig. 2. Microscopic analysis of SOCE in APP-producing Jurkat cells. (**A**) SOCE measurements in Fura-4F-loaded Jurkat cells that produced APP ($n = 13$), APP_{SWE} ($n = 12$) and control cells with an empty cassette ($n = 13$). (**B**) SOCE measurements in Jurkat cells that produced dominant-negative Orai1 (Orai1 DN; $n = 5$) and control cells ($n = 5$). Shown are averaged traces from representative experiments and calculated mean values with standard error. Differences from control cells were analyzed using unpaired *t*-test, and significant differences are marked with asterisks (***$p < 0.001$).

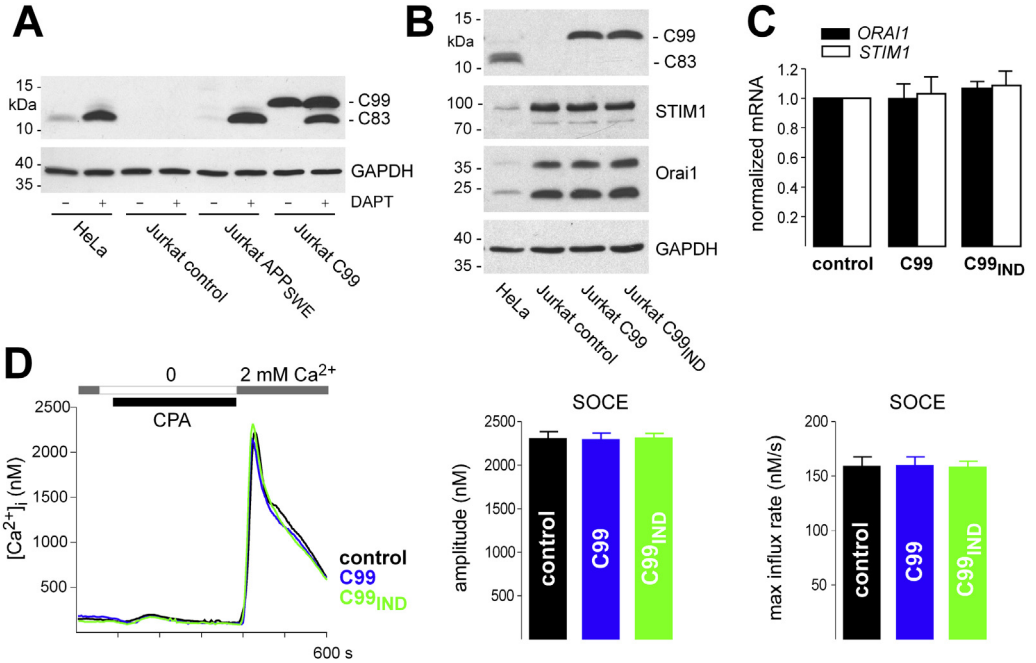

Fig. 3. Analysis of SOCE in Jurkat cells producing C99 fragments. (**A**) Immunoblot of small APP fragments (detected with Y188 antibody) in Jurkat cells stably expressing *APP_{SWE}*, C99 cDNA, or an empty cassette (control) compared with wildtype HeLa cells. DAPT treatment (5 μM for 5 h) is indicated below the gels. (**B**) Immunoblot of APP, Orai1, and STIM1 in Jurkat cells stably expressing C99 cDNA, $C99_{IND}$ cDNA, or an empty cassette (control) compared with wildtype HeLa cells. (**C**) qPCR analysis of *ORAI1* and *STIM1* mRNA levels in C99-producing Jurkat cells relative to those in Jurkat control cells. Differences were analyzed using one-sample *t*-test ($n = 3$ each). (**D**) SOCE measurements in Fura-4F-loaded Jurkat C99 cells ($n = 11$), $C99_{IND}$ cells ($n = 11$) and control cells ($n = 12$). Traces are from representative experiments. The data were analyzed using unpaired *t*-test.

through SOCs, utilizing the above-described protocol. The measurements showed no significant differences between Jurkat control cells and C99 or $C99_{IND}$ cells in SOCE amplitudes, maximal Ca^{2+} influx rates (Fig. 3D), or decline rates (Supplementary Fig. 1B).

3.5. Knockdown of APP in HeLa cells has no effect on SOCE

To further explore whether APP affects Ca^{2+} influx via SOCs, we switched to a loss-of-function approach. The *APP* expression in HeLa cells was knocked down by RNA interference. In these cells

(APP KD), *APP* mRNA levels were reduced 20-fold relative to the levels in cells with control shRNA (Fig. 1B), with concomitant severe depletion of the protein (Fig. 1A). Upon depletion of ER Ca^{2+} stores with CPA, we did not detect any significant differences in the amplitude or in the maximal influx rate of SOCE between Fura-2-loaded HeLa APP KD cells and control cells (Fig. 4A). The same results were obtained with HeLa cells transduced with viruses carrying another set of *APP*-targeting and control shRNAs (Supplementary Fig. 2). In parallel, we used HeLa cells with *ORAI1* knockdown (ORAI1 KD), and observed almost complete elimination of SOCE (Fig. 4A). Therefore, SOCE appeared to be strictly Orai1-dependent in HeLa cells. The quantification of *STIM1* and *ORAI1* mRNA levels did not reveal any significant differences between HeLa APP KD cells and control cells (Fig. 4B). In HeLa ORAI1 KD cells, *STIM1* mRNA levels remained unchanged, whereas *ORAI1* mRNA levels were reduced, as expected, but only five-fold (Fig. 4B). However, this moderate knockdown was sufficient to exert a profound effect on SOCE (Fig. 4A). In sum, these results indicate that APP is dispensable for SOCE upon complete ER Ca^{2+} store depletion in HeLa cells, and corroborate our results obtained with the gain-of-function approach in Jurkat cells.

4. Discussion

The present study utilized gain-of-function and loss-of-function approaches in cultured cells to shed light on the involvement of APP in SOCE. Specifically, we used Jurkat cells because they have (*i*) undetectable levels of APP, meaning no interference with ectopically expressed APP variants, (*ii*) small ER Ca^{2+} stores, which facilitates their depletion for SOCE measurements, and (*iii*) high expression of SOCE machinery (STIM1/Orai1), resulting in a large influx of Ca^{2+}. Prominent SOCE makes the quantification of Ca^{2+} influx a reliable readout of SOC activity, because it is less likely to be affected by other Ca^{2+} influx or extrusion mechanisms. Therefore, compared to cells with more complex Ca^{2+} handling machinery such as neurons, they constitute a simplified cell system that is well suited to analyzing this particular Ca^{2+} response. Although STIM1 and Orai1 proteins are sufficient for SOCE, several proteins have been recently shown to modulate it [26]. By analogy, we hypothesized that APP or its FAD mutants can affect the properties or levels of SOCE machinery. However, using fluorescent calcium indicators we did not detect any changes in the CPA-induced SOCE upon expression of APP or APP_{SWE} in Jurkat cells. Overproduction of C99 or $C99_{IND}$ fragments, with the aim to mimic amyloidogenic processing of APP, also had no effect. These results were corroborated by unchanged SOCE in HeLa cells with APP knockdown. Consistent with this, we also found no evidence for APP-dependent changes in the mRNA or protein levels of Orai1 and STIM1 in the analyzed cells.

Our results showing no involvement of APP in SOCE are in agreement with previous reports. APP overproduction was found to have no effect on SOCE induced by SERCA inhibition (with CPA or thapsigargin) in astrocytes, CHO and neuroblastoma cells [11,20,23], and APP FAD mutants had no effect on UTP-induced SOCE in PC12 cells [22]. However, the utilized cells expressed endogenous APP, which could obscure the molecular phenotype of ectopic APP. This problem was alleviated in our experimental model based on Jurkat cells. Similarly to what we report here for HeLa cells, SOCE was unchanged in hippocampal neurons lacking APP [9]. In contrast to these findings, Linde et al. found a clearly reduced SOCE in astrocytes with the *App* gene knock-out [20]. The observed reduction was attributed to decreased levels of TRPC1, a channel that contributes to astroglial SOCE [20]. Finally, two studies presented data for the role of APP harboring the Swedish mutation. Whereas Niu et al. reported augmentation of SOCE in neural 2a cells [21], a recent study found an attenuation of SOCE in hippocampal neurons isolated from FAD-APP knock-in mice [19]. The latter effect was attributed to increased levels of Aβ, resulting in overfilled ER Ca^{2+} stores, compensatory downregulation of STIM2 expression and impaired neuronal SOCE. The proposed role of STIM2 in hippocampal SOCE complies with the elevated STIM2/STIM1 ratios in the hippocampus as compared to other brain regions [28]. The results of the present study together with the findings of others suggest that APP and APP FAD mutants do not directly modulate SOCE mediated by STIM1 and Orai channels, but they may affect SOCE responses that rely on other proteins such as STIM2 or TRPC channels. In contrast, PS1 FAD mutations were shown to reduce SOCE in numerous cell types, both of neuronal and non-neuronal origin, although even with PS1 FAD mutants it is not clear whether they influence SOCs directly or act indirectly by changing the ER Ca^{2+} filling state [10,13]. Irrespective of exact targets, the more consistent effects of FAD-PS1 expression may be explained by the dual mode of action of PS1 that appears to involve not only the γ-cleavage of APP but also γ-secretase independent mechanisms. Nearly identical changes in neuronal Ca^{2+} handling and spine morphology have been recently reported by one laboratory for FAD-APP knock-in mice that strongly accumulated humanized Aβ, and for FAD-PS1 knock-in mice that lacked human Aβ altogether [13,19].

In summary, our data indicate that APP, APP_{SWE} mutant and amyloidogenic processing fragments do not influence STIM1/Orai1 levels or Orai-mediated SOCE upon complete ER Ca^{2+} store depletion. This contrasts with the relatively well-documented effect of PS1 on SOCE. Our results contribute to a better understanding of Ca^{2+}-related functions of FAD-linked proteins.

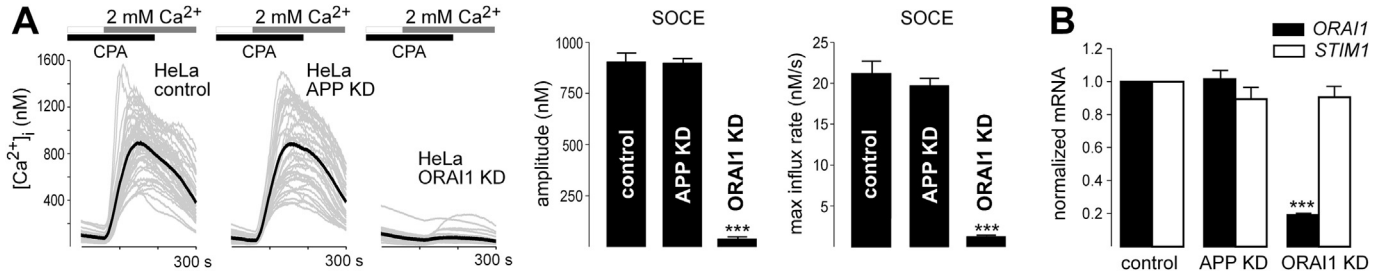

Fig. 4. Analysis of SOCE in HeLa cells depleted of APP. (**A**) SOCE measurements in Fura-2-loaded HeLa cells stably expressing *APP*-targeting shRNA (APP KD; $n = 8$), *ORAI1*-targeting shRNA (ORAI1 KD; $n = 3$) and control shRNA (control; $n = 8$). The stores were depleted with 20 μM CPA in Ca^{2+}-free buffer containing 0.5 mM EGTA for 400 s, and SOCE was initiated by the re-addition of 2 mM Ca^{2+}. Shown are averaged (black) and individual (gray) SOCE traces from representative experiments. The data were analyzed using unpaired *t*-test, and significant differences from controls are marked with asterisks (***$p < 0.001$). (**B**) qPCR analysis of *ORAI1* and *STIM1* mRNAs in cells presented in (A). Differences from the reference level of 1 set for controls were analyzed using one-sample *t*-test ($n = 3$ each). Statistical significance is marked with asterisks (***$p < 0.001$).

Acknowledgments

We thank D. Trono, D. Selkoe, T. Young-Pearse and A. Rao for plasmids. This work was supported by the Polish National Science Centre [grant 2011/03/B/NZ3/01760].

Transparency document

Transparency document related to this article can be found online at http://dx.doi.org/10.1016/j.bbrc.2016.08.072.

Appendix A. Supplementary data

Supplementary data related to this article can be found at http://dx.doi.org/10.1016/j.bbrc.2016.08.072.

References

[1] L.M. Bekris, C.E. Yu, T.D. Bird, et al., Genetics of Alzheimer disease, J. Geriatr. Psychiatry Neurol. 23 (2010) 213–227.
[2] D.J. Selkoe, Alzheimer's disease: genes, proteins, and therapy, Physiol. Rev. 81 (2001) 741–766.
[3] B. De Strooper, T. Iwatsubo, M.S. Wolfe, Presenilins and gamma-secretase: structure, function, and role in Alzheimer Disease, Cold Spring Harb. Perspect. Med. 2 (2012) a006304.
[4] S. Chakroborty, G.E. Stutzmann, Calcium channelopathies and Alzheimer's disease: insight into therapeutic success and failures, Eur. J. Pharmacol. 739 (2014) 83–95.
[5] M.J. Berridge, Calcium hypothesis of Alzheimer's disease, Pflugers Arch. 459 (2010) 441–449.
[6] L. Bojarski, J. Herms, J. Kuznicki, Calcium dysregulation in Alzheimer's disease, Neurochem. Int. 52 (2008) 621–633.
[7] K. Honarnejad, J. Herms, Presenilins: role in calcium homeostasis, Int. J. Biochem. Cell Biol. 44 (2012) 1983–1986.
[8] E. Popugaeva, I. Bezprozvanny, Role of endoplasmic reticulum Ca2+ signaling in the pathogenesis of Alzheimer disease, Front. Mol. Neurosci. 6 (2013) 29.
[9] J. Herms, I. Schneider, I. Dewachter, et al., Capacitive calcium entry is directly attenuated by mutant presenilin-1, independent of the expression of the amyloid precursor protein, J. Biol. Chem. 278 (2003) 2484–2489.
[10] M.A. Leissring, Y. Akbari, C.M. Fanger, et al., Capacitative calcium entry deficits and elevated luminal calcium content in mutant presenilin-1 knockin mice, J. Cell Biol. 149 (2000) 793–798.
[11] A.S. Yoo, I. Cheng, S. Chung, et al., Presenilin-mediated modulation of capacitative calcium entry, Neuron 27 (2000) 561–572.
[12] L. Bojarski, P. Pomorski, A. Szybinska, et al., Presenilin-dependent expression of STIM proteins and dysregulation of capacitative Ca2+ entry in familial Alzheimer's disease, Biochim. Biophys. Acta 1793 (2009) 1050–1057.
[13] S. Sun, H. Zhang, J. Liu, et al., Reduced synaptic STIM2 expression and impaired store-operated calcium entry cause destabilization of mature spines in mutant presenilin mice, Neuron 82 (2014) 79–93.
[14] C.R. Shideman, J.L. Reinardy, S.A. Thayer, Gamma-Secretase activity modulates store-operated Ca2+ entry into rat sensory neurons, Neurosci. Lett. 451 (2009) 124–128.
[15] Y. Akbari, B.D. Hitt, M.P. Murphy, et al., Presenilin regulates capacitative calcium entry dependently and independently of gamma-secretase activity, Biochem. Biophys. Res. Commun. 322 (2004) 1145–1152.
[16] P.G. Hogan, A. Rao, Store-operated calcium entry: mechanisms and modulation, Biochem. Biophys. Res. Commun. 460 (2015) 40–49.
[17] A. Verkhratsky, R.C. Reyes, V. Parpura, TRP channels coordinate ion signalling in astroglia, Rev. Physiol. Biochem. Pharmacol. 166 (2013) 1–22.
[18] L. Majewski, J. Kuznicki, SOCE in neurons: signaling or just refilling? Biochim. Biophys. Acta 1853 (2015) 1940–1952.
[19] H. Zhang, L. Wu, E. Pchitskaya, et al., Neuronal store-operated calcium entry and mushroom spine loss in amyloid precursor protein knock-in mouse model of Alzheimer's disease, J. Neurosci. 35 (2015) 13275–13286.
[20] C.I. Linde, S.G. Baryshnikov, A. Mazzocco-Spezzia, et al., Dysregulation of Ca2+ signaling in astrocytes from mice lacking amyloid precursor protein, Am. J. Physiol. Cell Physiol. 300 (2011) C1502–C1512.
[21] Y. Niu, Z. Su, C. Zhao, et al., Effect of amyloid beta on capacitive calcium entry in neural 2a cells, Brain Res. Bull. 78 (2009) 152–157.
[22] E. Stieren, W.P. Werchan, A. El Ayadi, et al., FAD mutations in amyloid precursor protein do not directly perturb intracellular calcium homeostasis, PLoS One 5 (2010) e11992.
[23] M. Chatzistavraki, E. Kyratzi, A. Fotinopoulou, et al., Downregulation of AbetaPP enhances both calcium content of endoplasmic reticulum and acidic stores and the dynamics of store operated calcium channel activity, J. Alzheimers Dis. 34 (2013) 407–415.
[24] G. Konig, U. Monning, C. Czech, et al., Identification and differential expression of a novel alternative splice isoform of the beta A4 amyloid precursor protein (APP) mRNA in leukocytes and brain microglial cells, J. Biol. Chem. 267 (1992) 10804–10809.
[25] K. Laky, W. Annaert, B.J. Fowlkes, Amyloid precursor family proteins are expressed by thymic and lymph node stromal cells but are not required for lymphocyte development, Int. Immunol. 21 (2009) 1163–1174.
[26] P.J. Shaw, B. Qu, M. Hoth, et al., Molecular regulation of CRAC channels and their role in lymphocyte function, Cell. Mol. Life Sci. 70 (2013) 2637–2656.
[27] Y. Gwack, S. Srikanth, S. Feske, et al., Biochemical and functional characterization of Orai proteins, J. Biol. Chem. 282 (2007) 16232–16243.
[28] A. Skibinska-Kijek, M.B. Wisniewska, J. Gruszczynska-Biegala, et al., Immunolocalization of STIM1 in the mouse brain, Acta Neurobiol. Exp. (Wars) 69 (2009) 413–428.